Turkish Journal of Chemistry

http://journals.tubitak.gov.tr/chem/

Research Article

Turk J Chem
(2019) 43: 948 – 962
© TÜBİTAK
doi:10.3906/kim-1810-72

Enhanced uptake capacities and isosteric heats of CO_2 and CH_4 adsorption on spent coffee ground activated carbons loaded with metal ions

Çisem KIRBIYIK[1], **Burak Zafer BÜYÜKBEKAR**[2,3,*], **Mahmut KUŞ**[4], **Mustafa ERSÖZ**[3,5]

[1]Department of Chemical Engineering, Faculty of Natural Sciences and Engineering, Konya Technical University, Konya, Turkey

[2]Department of Nanotechnology and Advanced Materials, Selçuk University, Turkey

[3]Advanced Technology Research and Application Center, Selçuk University, Konya, Turkey

[4]Institute of Energy Technologies, Gebze Technical University, Gebze, Turkey

[5]Department of Chemistry, Faculty of Science, Selçuk University, Konya, Turkey

Received: 31.10.2018 • **Accepted/Published Online:** 08.04.2019 • **Final Version:** 11.06.2019

Abstract: Low-cost activated carbon (AC) samples obtained from waste coffee grounds were used for CO_2 and CH_4 adsorption. ACs were prepared by chemical activation and carbonized at three different temperatures. AC carbonized at 800 °C showed a relatively high surface area (582.92 $m^2\ g^{-1}$) and high adsorption capacities of 2.6 mmol g^{-1} and 1.1 mmol g^{-1} at 25 °C for CO_2 and CH_4, respectively. Adsorbent samples were prepared by loading of Fe^{3+} metal ions onto ACs and their adsorption capacities were compared with those of nonloaded ACs. As expected, the loading of Fe^{3+} metal ions increased the adsorption capacities at all temperatures and the adsorption capacity of Fe^{3+}-loaded AC carbonized at 800 °C was 3.1 mmol g^{-1} for CO_2 and 1.2 mmol g^{-1} for CH_4 at 25 °C. The isosteric heats of adsorption were calculated at 0–35 °C with the range of 20–35 kJ mol^{-1} and 18–23 kJ mol^{-1} for CO_2 and CH_4, respectively. According to our findings, bio-based ACs can be used as an effective and alternative adsorbent for capturing different gas molecules.

Key words: Bio-based activated carbon, CO_2 adsorption, CH_4 adsorption, isosteric heat

1. Introduction

According to a World Meteorological Organization report, the concentrations of greenhouse gases, which play a critical role in global warming and the acidity of water sources, reached new highs in 2015.[1] That study reported that the global abundances of CO_2, CH_4, and N_2O gases were 400 ppm, 1845 ppb, and 328 ppb, respectively.[1] The main reason for the increasing concentrations of these gases in the atmosphere is the combustion of fossil fuels for transportation and to supply the energy demand.[2] As energy demand increases, the anthropogenic gas emissions increase every year; therefore, the capturing and storing of these gases have attracted attention in academic and industrial fields.[3] Different techniques for the capturing of greenhouse gases such as membrane separation, chemical absorption, or physical adsorption have been widely studied and reported.[4] In these techniques, adsorption has become one of the most promising techniques due to its facile application, low cost, and low energy requirement.[5]

In the adsorption technique, activated carbon (AC) is the most investigated adsorbent owing to its high adsorption capacity, high surface area, and porous structure.[6] However, AC is relatively expensive and this

*Correspondence: buyukbekar@gmail.com

limits the application of large-scale industrial operations.[7] Therefore, many studies have been reported to identify new low-cost and feasible precursor materials to reduce the production cost of AC.[8] Many different natural materials such as by-products of oil factories, solid and unwanted agricultural by-products, coal, and municipal waste have been investigated as precursors and evaluated in different adsorption processes.[9−14] As is well known, the natural chemical composition of a precursor material plays a crucial role in the adsorption capacity and application area of AC. In particular, AC species containing nitrogen are important for gas phase adsorption processes.[15,16] The presence of hetero atoms like nitrogen on the surface of carbon improves the surface polarity and basicity, leading to enhancement of the interaction between adsorbent surface and gas molecules with an acidic nature like CO_2 and CH_4. For this reason, spent coffee grounds (GC) were selected as a precursor to produce AC. This municipal waste contains caffeine ($C_8H_{10}N_4O_2$), which is a natural source of nitrogen, and it is produced in large amounts in modern life. There have been many reports about the adsorption of different pollutants such as dyes and phenols onto GC-based AC, but there are surprisingly limited studies on the adsorption of different types of gas pollutants.[17] Therefore, we discuss here the production of low-cost and highly effective activated carbon (GCAC) from spent coffee grounds for the adsorption of CO_2 and CH_4 gases. In addition to the importance of the nature of the precursor material and the structural properties, the modification of AC's surface has an important effect on the gas adsorption capacity. The modification procedure provides an opportunity to incorporate surface functional groups with improved affinity for increased gas adsorption performance. Even though the role of metal ion loading to the AC surface in gas adsorption still needs to be explored, it is considered that the basic nature of metals can interact with acidic CO_2 and CH_4 molecules. Therefore, we also investigated the effect of loading Fe^{3+} metal ions onto AC on adsorption capacity.

AC samples can be produced by chemical or physical activation. $ZnCl_2$, a typical kind of Lewis acid, can be utilized as a chemical activation agent to produce AC with a high surface area. $ZnCl_2$ has been reported to promote dehydration during the carbonization process, contributing to the development of pore structure. At higher temperatures, $ZnCl_2$ vaporizes and decomposes into zinc and chlorine to create an enlarged pore structure. To produce highly efficient bio-based AC, GC was chemically activated by $ZnCl_2$ and then the effects of carbonization temperature (600, 700, and 800 °C) on surface characteristics and gas adsorption capacities were examined. The produced GCAC samples were treated with a certain volume of Fe^{3+} metal ion solution. The effect of loading Fe^{3+} metal ions onto the GCAC produced (Fe-GCAC) was investigated. We determined that the Fe^{3+} metal ions-loaded Fe-GCAC sample carbonized at 800 °C shows an effective increase of 4.2 mmol g^{-1} adsorbed CO_2 in comparison with 3.5 mmol g^{-1} adsorbed CO_2 onto the GCAC sample produced at the same temperature without metal ion loading at 0 °C under 900 mmHg adsorption conditions. A similar trend in the same samples was observed for the adsorption of CH_4 with an increase from 1.5 mmol g^{-1} to 1.7 mmol g^{-1}. Finally, the recoverability of the best resulting adsorbent was tested after the adsorption study. The results obtained show that the AC from natural waste sources is applicable for future gas adsorption applications. The CO_2 and CH_4 adsorption capacities can be enhanced by adding a simple step to the production process of ACs via loading metal ions.

2. Experimental

2.1. Materials and instrumentation

All chemicals were purchased from commercial sources and used without further purification. Waste coffee grounds chosen as precursor were collected from domestic coffee machines. Deionized water with a specific

resistance of 18.2 MΩ cm was obtained by ion exchange and filtration (Direct-Q Water Purification System). $ZnCl_2$ pellets (98%) and iron (III) chloride hexahydrate (98%) were purchased from Sigma-Aldrich.

Morphological, structural, and surface analyses were carried out using Fourier transform infrared spectroscopy (FTIR, Bruker Vertex 70), a scanning electron microscope (SEM, Zeiss EVO 50), thermal gravimetric analysis (TGA, Mettler Toledo TGA/DSC 2), and Brunauer–Emmett–Teller (BET, Micromeritics Tristar II) techniques.

2.2. Preparation of activated carbons

The preparation method for GCAC and Fe-GCAC samples obtained at different temperatures from GC is given in the Scheme. The GC was washed with distilled water, dried at room temperature, and subsequently dried in an oven at 85 °C for 48 h to remove its moisture. GCAC samples were prepared by two-step chemical activation and carbonization as reported previously.[18,19] For the chemical activation of precursor, a certain amount of $ZnCl_2$ pellets was dissolved in double deionized water and an equal amount of GC was immersed into $ZnCl_2$ solution for impregnation. The impregnated biomass samples were kept at room temperature overnight and subsequently dried in an oven at 85 °C for 48 h. Dried samples were carbonized at three different final temperatures (600, 700, and 800 °C) with a 10 °C/min heating rate. After cooling down to room temperature, samples carbonized (coded as GCAC/600, GCAC/700, and GCAC/800 according to activation temperature) were washed with distilled water several times to remove residuals and then dried at 85 °C for 48 h.

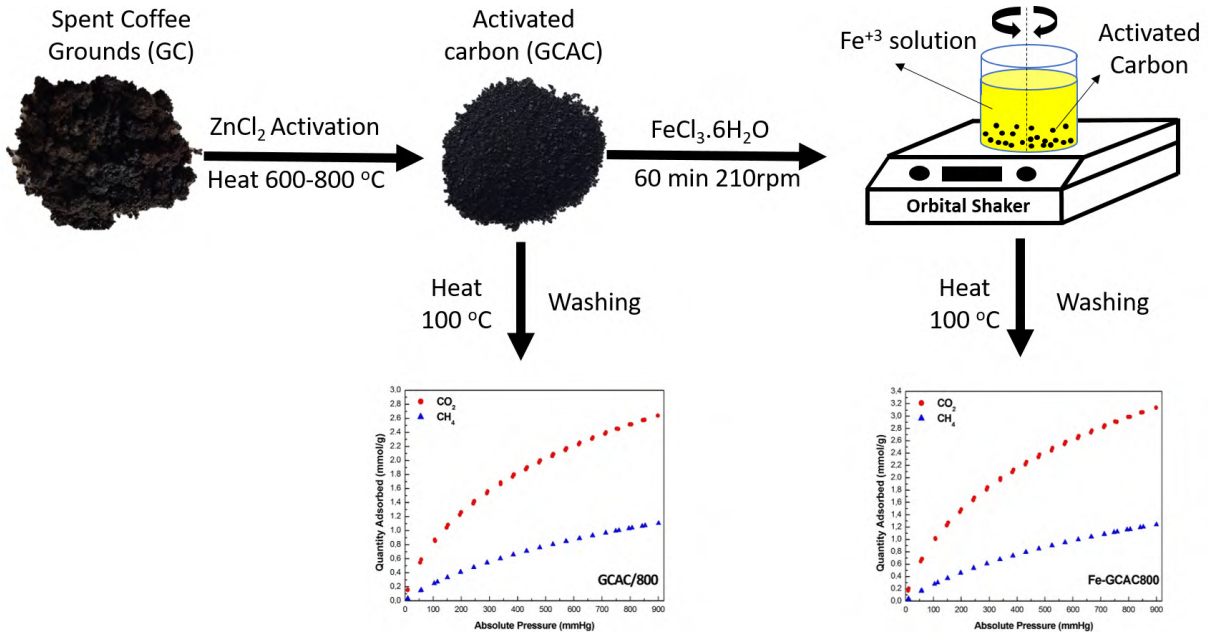

Scheme. The preparation method of GCAC and Fe-GCAC samples from GC.

In order to determine the adsorption capacities of Fe^{3+} metal ions-loaded GCAC samples, Fe-GCAC samples were prepared by treating 0.4 g of each GCAC sample with 400 mL of 400 mg/L of Fe^{3+} solution for 60 min. After metal ion loading, each Fe-GCAC sample was separated by filtering and washed with deionized water to remove nonadsorbed Fe^{3+} ions, followed by drying at 85 °C for 24 h.

2.3. Material characterizations

The thermogravimetric analyses of raw material and $ZnCl_2$ impregnated raw material ($ZnCl_2$-GC) and two ACs as representative samples were performed. Raw material, $ZnCl_2$-GC, GCAC, and Fe-GCAC samples produced at three different temperatures were examined using FTIR to determine their surface chemistry. The surface and pore texture of AC samples were characterized using an adsorption apparatus at –196 °C by measuring N_2 adsorption–desorption isotherms. The surface area and average pore width were calculated by the BET method. Total pore volume was obtained from N_2 adsorption at the highest relative pressure studied. The average pore diameter was calculated by the Barrett–Joyner–Halenda (BJH) method. Before the adsorption analysis, the adsorbents were degassed at 300 °C overnight to remove moisture and other adsorbed gases. In order to determine the surface morphology of AC samples, SEM was used via the conventional method including mounting the adsorbent samples on an aluminum stub.

2.4. CO_2 and CH_4 adsorption–desorption and recoverability experiments

CO_2 and CH_4 adsorption–desorption measurements were carried out using the same apparatus used in the N_2 adsorption experiments. All gas adsorption–desorption experiments were performed with pure gases. The adsorption–desorption isotherms of both CO_2 and CH_4 for all samples degassed at 300 °C were measured up to 900 mmHg at 0, 25, and 35 °C.

The cyclic working capacity of CO_2 onto the sample with the highest adsorption capacity was performed for 6 cycles at 25 °C up to 760 mmHg to test the stability and adsorptive repeatability. After each cycle, saturated adsorbent was degassed at 300 °C in pure N_2 to fully release the adsorbed CO_2 overnight.

3. Results and discussion

3.1. Characterizations

Figure 1a shows TGA curves of GC and $ZnCl_2$-GC in air and N_2 atmosphere. The TGA curves of both samples showed similar weight loss stages, while the percent weight losses were different. The percent weight loss of $ZnCl_2$-GC was lower than that of raw material. Between 30 and 150 °C, raw material exhibited a weight loss of 22 wt.%, whereas $ZnCl_2$-impregnated raw material exhibited a weight loss of 7 wt.%. The first weight loss stage is attributed to physisorbed water and gases.[20] The significant weight losses observed are associated with the decomposition of hydroxyl, carboxylic, and other surface functional groups at the second weight loss stage from ∼200 to 500 °C.[21] Figure 1b shows the TGA analysis for GCAC/600 and Fe-GCAC/600 samples. Up to ∼100 °C, both samples exhibited a weight loss of ∼10 wt.% and, up to ∼500 °C, there were no significant weight changes. By analyzing both graphs, it can be observed that the AC samples are very highly resistant to weight loss compared to GC and $ZnCl_2$-GC from room temperature to 500 °C. The most significant weight loss of AC samples occurred between 500 and 1000 °C. Although both AC samples showed similar weight loss trends, Fe-GCAC/600 showed less weight loss than GCAC/600 did after the loading of Fe^{3+} ions.

The FT-IR spectra of raw material, $ZnCl_2$-impregnated sample, and all ACs produced are given in Figure 2. As expected, the broad bands at 3315 cm^{-1}, related to hydroxyl O–H from physiosorbed water, disappeared after carbonization. The bands observed at 2923 cm^{-1} and 2853 cm^{-1}, at 1743 cm^{-1}, at 1636 cm^{-1}, and at 1155 cm^{-1} are assigned to C–H stretching, C=O stretching in carboxylic groups, and N–H and C–N functional groups, respectively.[22,23] Therefore, it can be proposed that the prepared ACs are mainly composed of carbon and nitrogen containing functional groups. While these bands disappeared due to the decomposition of lignin

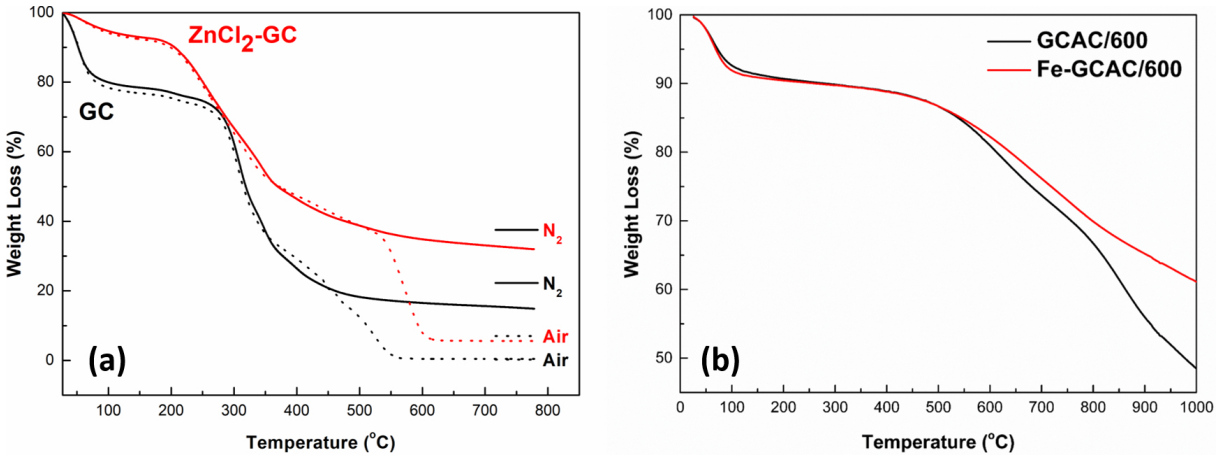

Figure 1. TGA spectra of (a) GC and $ZnCl_2$-GC and (b) GCAC/600 and Fe-GCAC/600.

content of raw material during carbonization, a new band appeared at 2357 cm^{-1} corresponding to an increase in nitrogenous groups in AC produced.[24] This is consistent with reports on the carbonization of nitrogen containing precursors to introduce nitrogen to carbonaceous materials.[25] Moreover, the broad bands at 670 cm^{-1} support the presence of Fe–O bonds.[26]

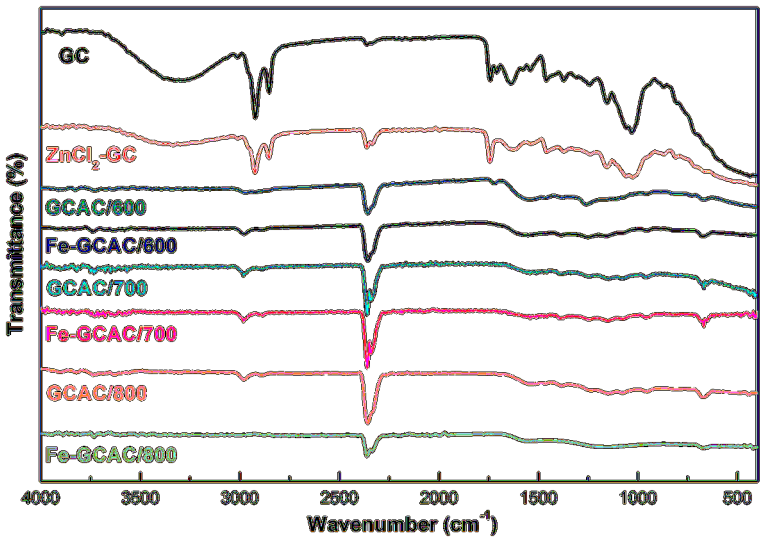

Figure 2. FT-IR spectra of GC, $ZnCl_2$-GC, and activated carbons produced.

Table 1 shows the textural characteristics and BET surface areas of all samples and they were derived from the N_2 adsorption and desorption isotherms given in Figure 3. All samples gave type I isotherms in the IUPAC classification, which indicates the microporous nature of samples. In addition, a small hysteresis is seen between the adsorption and desorption isotherms in Figure 3. It indicates that there are small proportions of mesopores and macropores.[27] BET specific surface areas of ACs were determined as 241.82, 446.87, and 582.92 $m^2\ g^{-1}$ for samples carbonized at 600, 700, and 800 °C, respectively. Compared with the literature, GCAC/800 showed a relatively high surface area. For example, Hao et al. reported that physically AC obtained from biosludge has a surface area of 489 $m^2\ g^{-1}$ (the comparison of surface areas of different ACs is given in

Table 2).[28–32] As carbonization temperature increased, the total pore volume exhibited an increase from 0.12 to 0.28 cm^3/g.

Table 1. Physical characteristics of adsorbents.

	GCAC/600	Fe-GCAC/600	GCAC/700	Fe-GCAC/700	GCAC/800	Fe-GCAC/800
BET surface area (m^2 g^{-1})	241.82	221.41	446.87	563.25	582.92	667.33
Total pore volume (cm^3 g^{-1})	0.119	0.108	0.215	0.271	0.280	0.321
Micropore volume (cm^3 g^{-1})	0.094	0.085	0.180	0.226	0.240	0.269
Average pore diameter (nm)	6.35	5.86	4.89	4.54	4.78	4.595
Average pore width (nm)	1.97	1.96	1.93	1.92	1.91	1.926

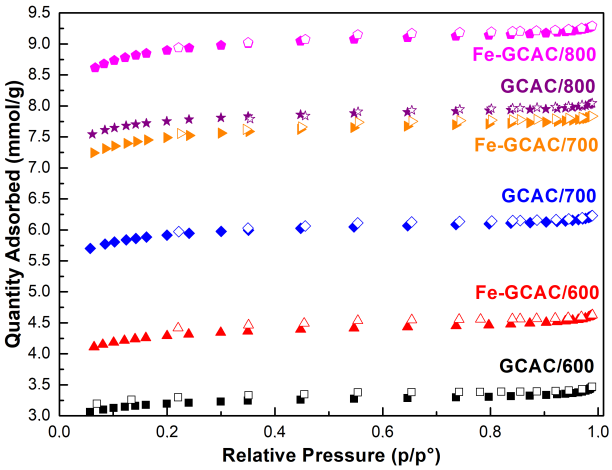

Figure 3. The N_2 adsorption and desorption isotherms of GC, $ZnCl_2$-GC, and activated carbons produced.

Table 2. Comparison of the physical characteristics of activated carbons obtained from different biomass materials.

Adsorbent	S_{BET} (m^2 g^{-1})	V_{total} (cm^3 g^{-1})	Pore size (nm)	References
Physically activated carbon from biosludge	489	0.39	-	[28]
Physically activated carbon from beer waste	622	0.32	-	
Raw-palm shell activated carbon	617	0.32	2.09	[29]
CO_2-palm shell activated carbon	623	0.31	2.02	
wt. 10% MgO loaded activated carbon from whitewood	651	0.34		[30]
microporous carbon compartments from pristine wheat flour	648	0.30	-	[31]
The aminated activated carbon (concentrated)	507	0.30	3.28	[32]
Fe-GCAC/800	667	0.32	4.59	*Present study*

As seen clearly from Table 1, the N_2 adsorption capacity is dramatically influenced by both carbonization temperature and metal ion loading onto ACs. After the loading of Fe^{3+} ions onto ACs, the BET surface areas and total pore volumes slightly increased. Regardless of Fe^{3+} ions content, treating AC samples with an excessive amount of metal ion solution leads to larger pore volumes and surface areas.[33] When the temperature increased from 600 to 800 °C, the surface areas of Fe^{3+} loaded ACs increased from 221 to 667 m^2/g as shown in Table 1. Accordingly, the high BET surface areas and large amount of N_2 adsorbed show that all samples are

suitable for effective elimination of air pollutants. SEM images of all samples show a typical morphology with a highly microporous structure (Figure 4). The morphological results are consistent with the results revealed from N_2 adsorption experiments. $ZnCl_2$ activation provided an orderly pore distribution and well-developed surface due to its acidic character. Its dehydration and impurity scraping effect produce open pores in the surface.[34–36]

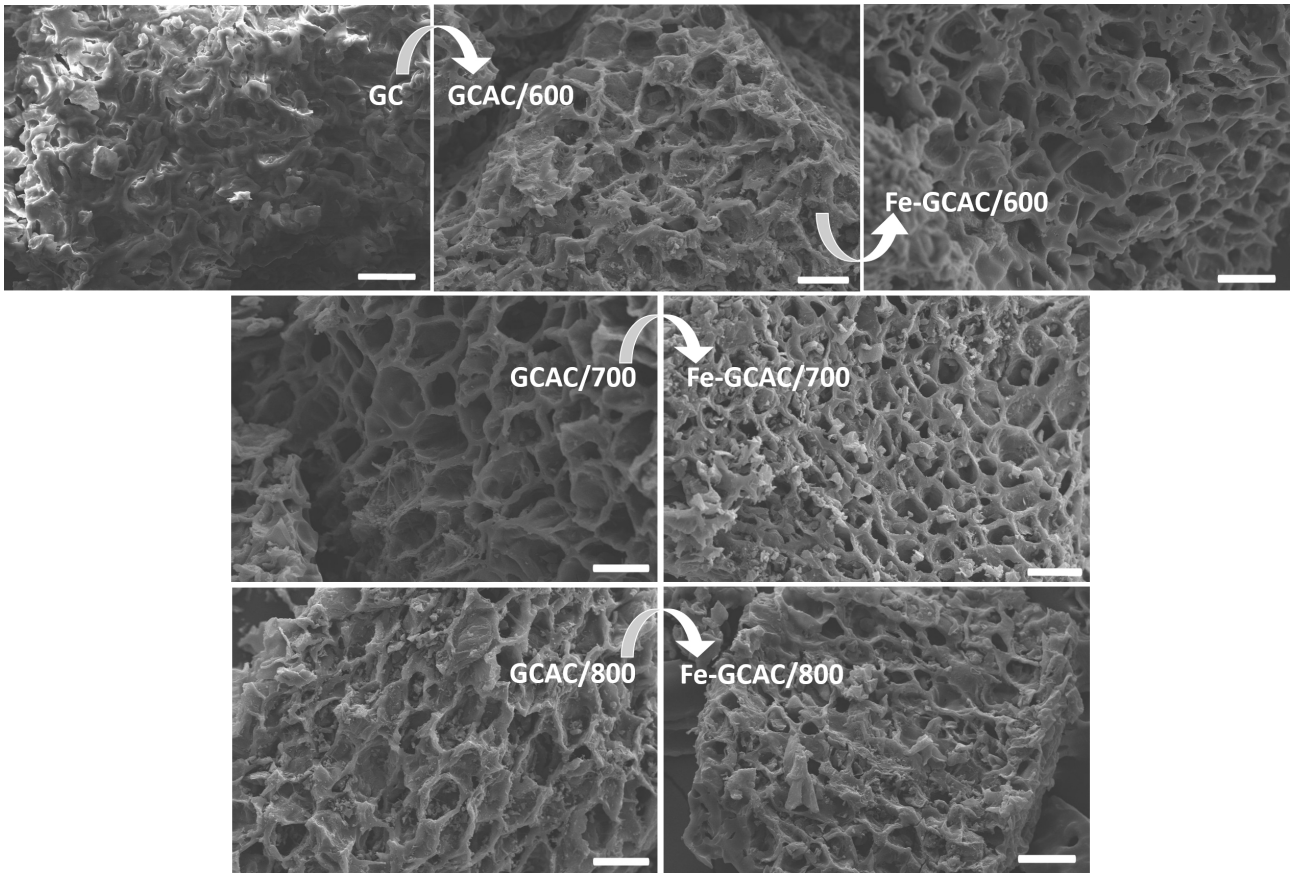

Figure 4. SEM images of raw material and all activated carbons produced (scale bar = 40 μm).

The pore size distribution and cumulative pore volumes were determined based upon the adsorption–desorption isotherm by a modified BJH model. Figure 5 shows the pore size distributions, which indicates that all samples have a unimodal pattern with a broad peak at 2.5?nm. As an exception, in Figure 5, there is also a remarkable peak at 110 nm in pore size distribution for the GCAC/600 sample. Pore volumes less than 10?nm dominate in all AC samples. The loading of Fe^{3+} ions onto ACs has no strong effect on the pore size distribution. Figure 6 is a plot of the cumulative pore volume of all AC samples. As seen, the cumulative pore volumes of nonloaded AC samples increased from 0.012 to 0.014 $cm^3\ g^{-1}$, whereas the cumulative pore volumes of AC samples loaded with Fe^{3+} metal ions increased from 0.010 to 0.018 $cm^3\ g^{-1}$ on increasing activation temperature from 600 to 800 °C. It can be said that the pores of the ACs were not blocked by Fe^{3+} ions, which is consistent with the findings in Table 1.

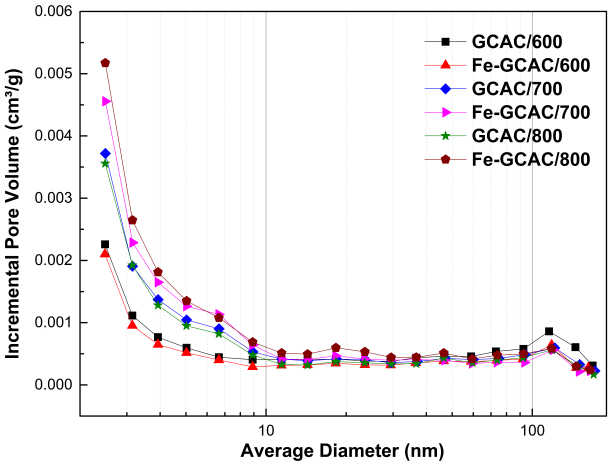

Figure 5. Incremental pore volumes of activated carbon samples.

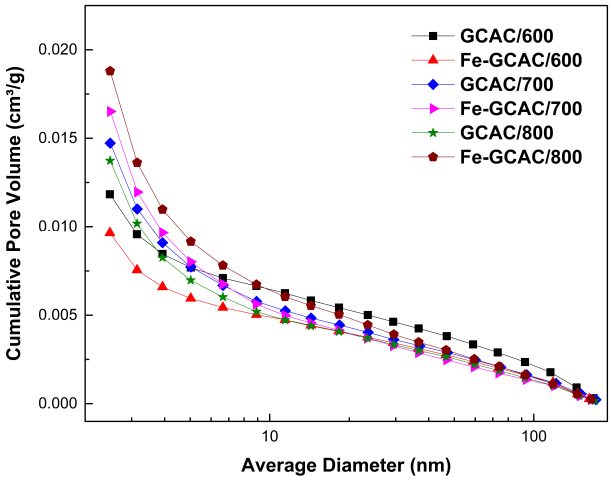

Figure 6. Cumulative pore volumes of activated carbon samples.

3.2. CO_2 and CH_4 adsorption–desorption

To produce highly efficient AC it is required to control the anthropogenic gas emission especially under ambient conditions.[37] CO_2 and CH_4 adsorption–desorption isotherms measured at 25 °C room temperature are shown in Figure 7. Table 3 lists CO_2 and CH_4 adsorption capacities of all samples at 0, 25, and 35 °C. In the case of metal ion-free samples, the amount of CO_2 adsorbed increased from 1.7 to 2.6 mmol g^{-1} when carbonization temperature increased. A similar trend was observed for CH_4 adsorption. The amount of CH_4 adsorbed onto the GCAC/800 sample was 1.1 mmol g^{-1}. When we compared Fe^{3+} metal ion-loaded samples with metal ion-free samples, loading of Fe^{3+} ions onto AC significantly increased the adsorption capacities at all carbonization temperatures. It can be explained by the increasing in chemisorption of gas molecules onto ACs, which is related to electrostatic interactions between CO_2–CH_4 and extra Fe^{3+} metal ions.[21,34,38] Fe-GCAC/800 showed a high CO_2 adsorption capacity of 3.1 mmol g^{-1}. This amount of CO_2 adsorbed is higher than that of many bio-based ACs studied in the literature. For instance, Plaza et al. produced AC from spent coffee grounds at a carbonization temperature of 600 °C with 1:1 ratio of KOH/precursor and the adsorbent exhibited a CO_2 adsorption capacity of 2.8 mmol g^{-1} at 25 °C and 1 bar.[39] Another study reported that the AC obtained using olive stone showed 2.4 mmol g^{-1} CO_2 adsorption capacity at the same adsorption conditions (for further comparisons of CO_2 and CH_4 adsorption capacities, see Table 4).[40–56] These results suggest that the addition of a single metal ion loading step into the AC production process can be used to improve the adsorption capacity of ACs.

There are many reports on the identification of the CO_2 and CH_4 adsorption behaviors of different ACs.[57,58] Table 3 shows the adsorption capacity results obtained in the present work at 0, 25, and 35 °C. CO_2 and CH_4 adsorption–desorption isotherms measured at 0 and 35 °C are shown in Figures 8 and 9, respectively. As shown in Table 3, Fe-GCAC/800 showed the highest CO_2 and CH_4 adsorption capacities of 4.2 and 1.7 mmol g^{-1} at 0 °C. When the temperature increased, the amount of adsorbed CO_2 decreased to 2.4 mmol g^{-1}, whereas the amount of adsorbed CH_4 decreased to 0.8 mmol g^{-1}. This shows that the adsorption is an exothermic process.[59]

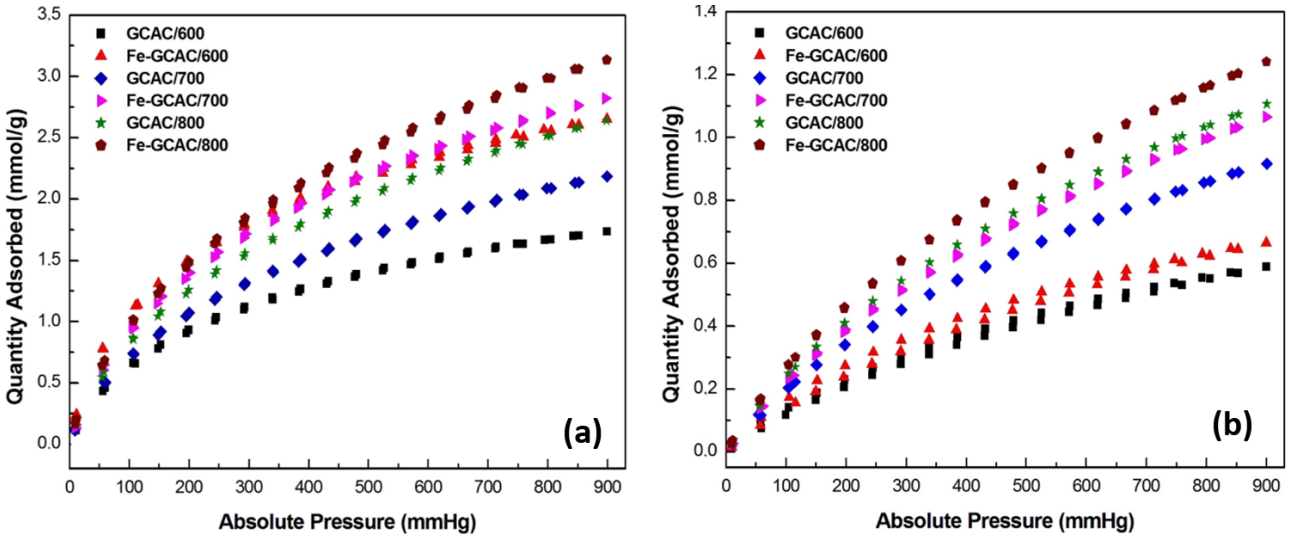

Figure 7. The (a) CO_2 and (b) CH_4 adsorption–desorption isotherms measured at 25 °C on activated carbons produced.

Table 3. Maximum CO_2 and CH_4 adsorption capacities at 0 °C, 25 °C, and 35 °C up to 900 mmHg.

Adsorption capacity ($mmol_{adsorbed}/g\ _{adsorbent}$)	Adsorption temperature	GCAC/600	Fe-GCAC/600	GCAC/700	Fe-GCAC/700	GCAC/800	Fe-GCAC/800
CO_2	0 °C	2.361	2.888	2.911	3.759	3.484	4.179
CH_4		0.860	0.939	1.219	1.523	1.468	1.699
CO_2	25 °C	1.734	2.652	2.184	2.823	2.641	3.138
CH_4		0.589	0.664	0.917	1.065	1.107	1.242
CO_2	35 °C	1.317	1. 675	1.578	2.218	1.904	2.379
CH_4		0.513	0.498	0.659	0.836	0.817	0.862

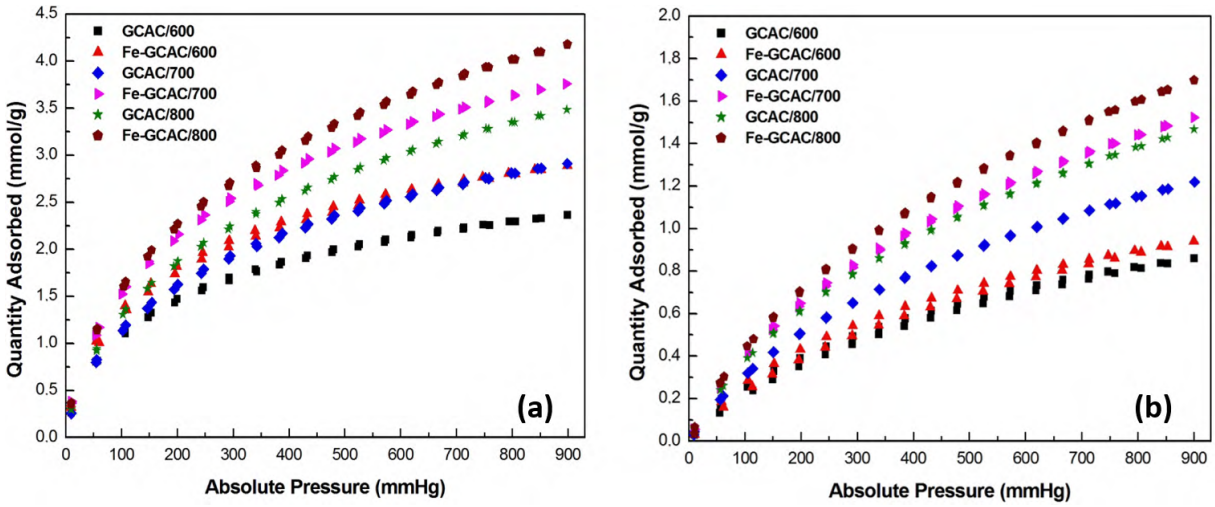

Figure 8. The (a) CO_2 and (b) CH_4 adsorption–desorption isotherms measured at 0 °C on activated carbons produced.

Table 4. Comparison of the adsorbed amount of CO_2 and CH_4 (at 25 °C) for porous carbons obtained from different biomass materials.

Adsorbent	CO_2 (mmol/g)	CH_4 (mmol/g)	References
Olive stone-a	2.4	-	[40]
Olive stone-b	3.0	-	[41]
Almond shells	2.7	-	
White wood	1.8	-	[42]
Almond shell	2.7	-	[43]
Microalgae	1.4	-	[44]
Coconut shell-a	4.0	1.2	[45]
Coconut shell-b	2.0	-	[46]
Resin	2.3	-	[28]
Grass cuttings	0.9	-	[47]
Resin	2.3	-	[48]
Pine cone	2.8	-	[49]
Borazine-linked polymers-1	-	0.5	[50]
Borazine-linked polymers-12	-	0.3	
Monolithic activated carbons	-	0.3	[51]
Sewage sludge	1.27 (30 °C)		[52]
Mango seed	1.20 (30 °C)	0.73 (30 °C)	[53]
Fungi	3.5		[54]
Rice husk	2.82		[55]
Cherry stones	1.63		[56]
Fe-GCAC/800	3.1	1.2	*Present study*

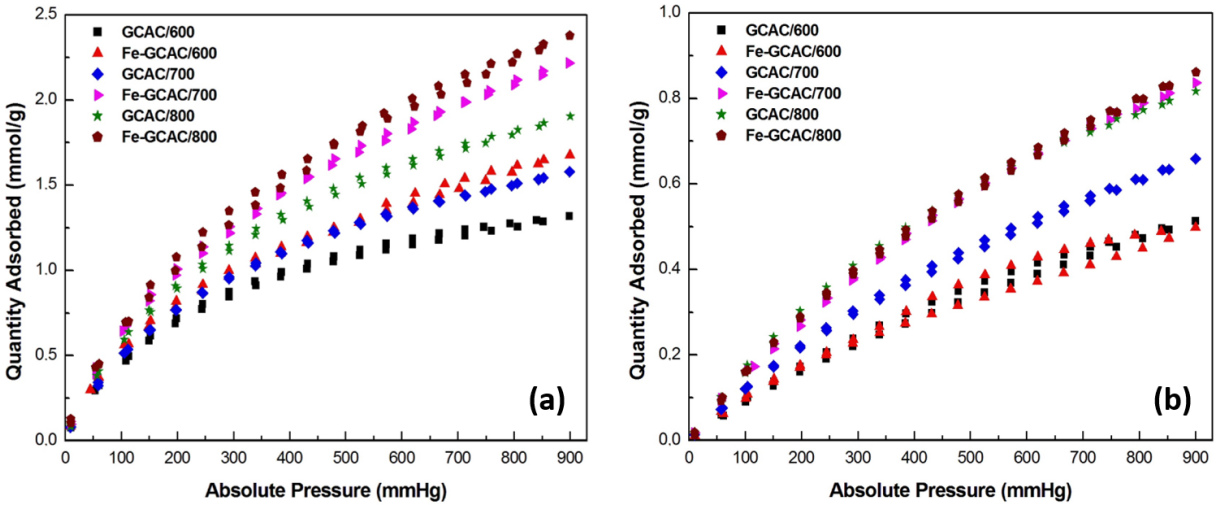

Figure 9. The (a) CO_2 and (b) CH_4 adsorption–desorption isotherms measured at 35 °C on activated carbons produced.

3.3. Isosteric heat of adsorption

The isosteric heat of adsorption was calculated by applying the Clausius–Clapeyron equation (Eq. (1)) to provide better understanding of the strength and type of interaction between ACs produced and adsorbate molecules.[60]

To calculate the isosteric heat of adsorption, adsorption isotherms were measured at three different temperatures (0, 25, and 35 °C).

$$Q_{st} = -R\left[\frac{\partial \ln p}{\partial\left(\frac{1}{T}\right)}\right]_q, \tag{1}$$

where Q_{st} is the isosteric heat of adsorption, R is the ideal gas constant, p is pressure, and T is temperature. Integration of Eq. (1) gives Eq. (2), as given below:

$$(\ln p)_q = -\left(\frac{Q_{st}}{R}\right)\left(\frac{1}{T}\right) + c, \tag{2}$$

where c is a constant. Q_{st} is calculated from the slope of the curve obtained by plotting ln p vs. 1/T. Figures 10a and 10b, 11a and 11b, and 12a and 12b show the variations in isosteric heat of CO_2 and CH_4 adsorption onto GCAC/600, Fe-GCAC/600, GCAC/700, Fe-GCAC/700, GCAC/800, and Fe-GCAC/800, respectively.

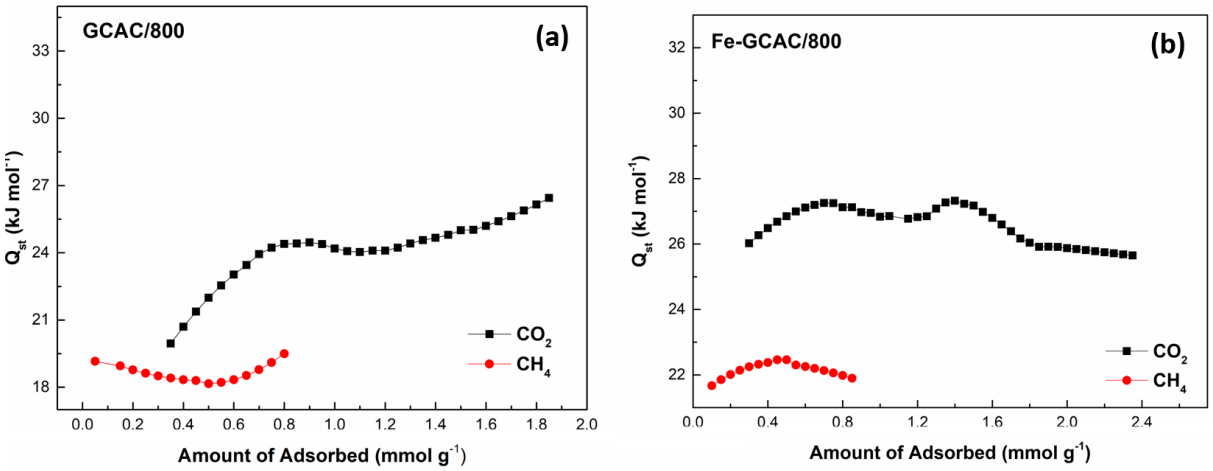

Figure 10. The CO_2 and CH_4 adsorption isosteres onto (a) GCAC/600 and (b) Fe-GCAC/600 samples at 0, 25, and 35 °C.

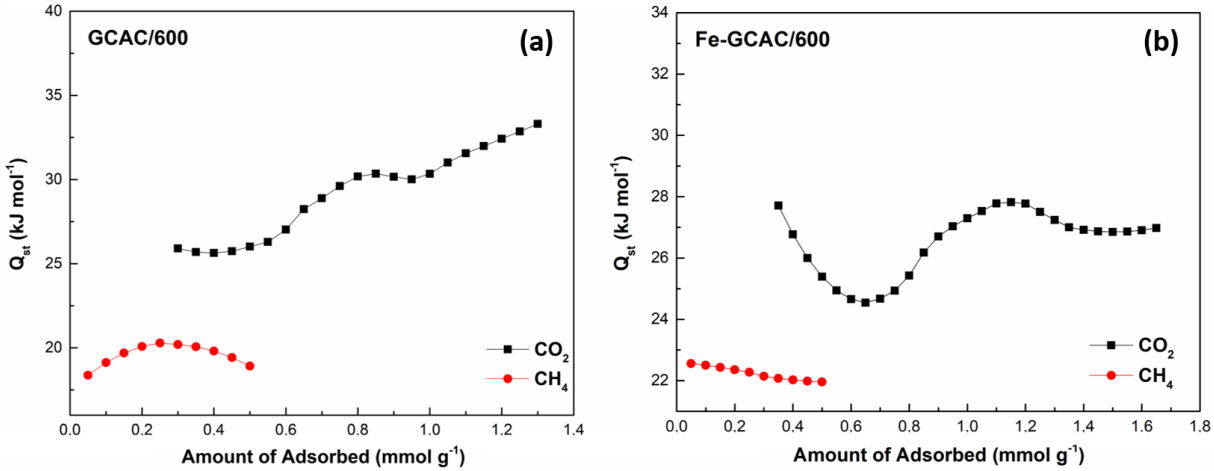

Figure 11. The CO_2 and CH_4 adsorption isosteres onto (a) GCAC/700 and (b) Fe-GCAC/700 samples at 0, 25, and 35 °C.

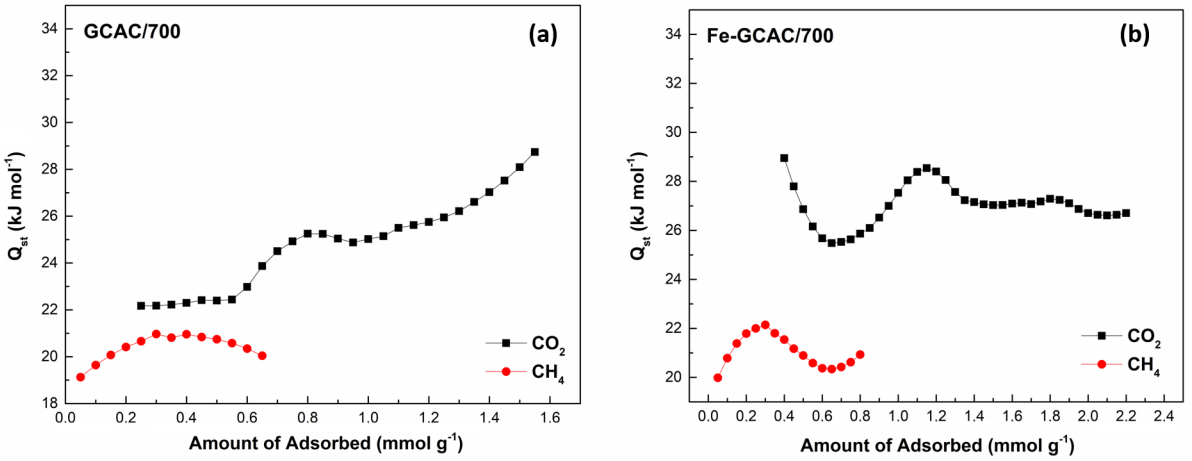

Figure 12. The CO_2 and CH_4 adsorption isosteres onto (a) GCAC/800 and (b) Fe-GCAC/800 samples at 0, 25, and 35 °C.

In the experimental results for all GCAC samples nonloaded with Fe^{3+} ions, it can be seen that the Q_{st} values of adsorption for CO_2 show an increase with increased CO_2 loading. In Figure 10a, Q_{st} values were calculated in the range of 26–32 kJ mol^{-1} for CO_2 at loadings of 0.2–1.3 mmol g^{-1} for GCAC/600, which is in accordance with the report data indicating that favorable interactions exist among adsorbed CO_2 molecules.[61] For GCAC/600, the Q_{st} value of CH_4 increased from 18 kJ mol^{-1} to 21 kJ mol^{-1} with increasing loading $<$0.3 mmol g^{-1}. After that, with increasing loading, the Q_{st} value of adsorption decreased from 21 to 19 kJ mol^{-1} up to 0.5 mmol g^{-1}. Similar behavior was reported by Khalili et al. for adsorption of CH_4 on pine cone-based AC.[62] For all GCAC samples loaded with Fe^{3+} ions, it can be seen that the Q_{st} values of CO_2 obtained were smaller than 30 kJ/mol, but there is a wave in the Q_{st} values as a function of surface loading. This fluctuation in the Q_{st} values can be attributed to different surface coverage values. The isosteric heat of adsorption depends on surface coverage.[63] For GCAC/800, Q_{st} values were calculated in the ranges of 20–27 kJ mol^{-1} for CO_2 at loadings of 0.3–1.8 mmol g^{-1} and 18–20 kJ mol^{-1} for CH_4 at loadings of 0.05–0.8 mmol g^{-1}. For Fe-GCAC/800, the values were calculated in the ranges of 25–28 kJ mol^{-1} for CO_2 at loadings of 0.3–2.4 mmol g^{-1} and 21–23 kJ mol^{-1} for CH_4 at loadings of 0.1–0.9 mmol g^{-1}. According to the general trend, the loading of Fe^{3+} ions onto the ACs increases the Q_{st} values calculated due to the electrostatic interactions between both CO_2–CH_4 and extra Fe^{3+} metal ions.[57] This increase agrees with the increase in adsorption capacity mentioned in Sec. 3.2. Q_{st} values calculated for CO_2 adsorption compare well with reported values on other different carbonaceous materials in the literature[64,65] and Q_{st} values calculated for CH_4 adsorption are similar to reported values.[66,67] For all samples, Q_{st} values were in a moderate range of 20–35 kJ mol^{-1} and 18–23 kJ mol^{-1} for CO_2 and CH_4, respectively. Since the Q_{st} values are relatively low, it can be considered that the interactions between gas molecules and AC samples predominantly proceed by physisorption.[68] The low Q_{st} values suggests the potential for recoverability and reusability of the adsorbents.[69] Therefore, the recoverability potential was investigated as described below.

3.4. Recoverability tests

Recoverability of adsorbent is one of the most important parameters for future practical applications of adsorption. To test the recoverability of ACs, multicycle CO_2 adsorption experiments were repeated six times

using Fe-GCAC/800 with the highest adsorption capacity by the same apparatus mentioned in Sec. 2.2 and detailed in Sec. 2.3. According to the results shown in Figure 13, only 2% adsorption capacity loss was observed after six cycles. This low loss of adsorption capacity is indicative of Fe-GCAC/800 recoverable with maintained adsorbent stability.

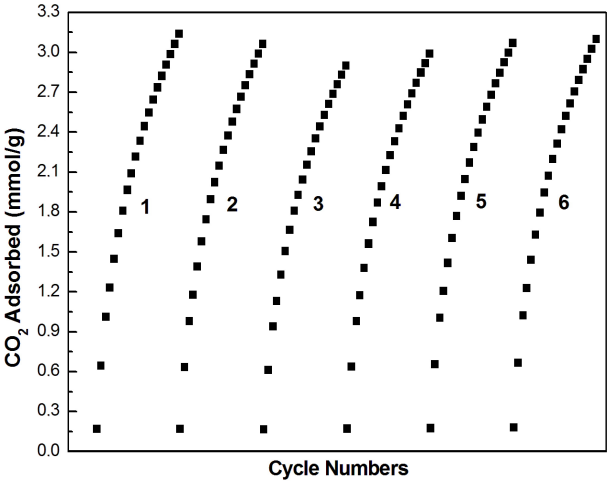

Figure 13. CO_2 adsorption cycles for Fe-GCAC/800 (repeating adsorption at 25 °C followed by desorption at 25 °C).

3.5. Conclusions

In this study, microporous ACs were prepared from spent coffee grounds via chemical activation with 1:1 ratio of $ZnCl_2$:GC and the mixture was carbonized at three different temperatures (600, 700, and 800 °C). The GCAC/800 sample showed the highest surface area of 583 m^2 g^{-1} when compared to metal ion-free AC samples. The ACs produced were used to capture CO_2 and CH_4. The GCAC/800 sample showed high adsorption capacities of 2.6 mmol g^{-1} and 1.1 mmol g^{-1} at 25 °C for CO_2 and CH_4, respectively. To investigate the effect of metal ion loading onto carbonaceous materials, the ACs produced were simply treated with a certain volume of Fe^{3+} metal ion solutions. The BET analysis and the gas adsorption experiments showed that surface areas and adsorption capacities increased with loading Fe^{3+} ions onto the ACs produced. The Fe-GCAC/800 sample with the highest surface area showed the maximum adsorption capacity of 3.1 mmol g^{-1} CO_2 and 1.2 mmol g^{-1} CH_4 at 25 °C. For all samples, the isosteric heat of adsorption was additionally calculated in the range of 20–35 kJ mol^{-1} and 18–23 kJ mol^{-1} for CO_2 and CH_4, respectively at 0, 25, and 35 °C. These low Q_{st} values calculated indicate that AC samples can be reused and have a potential for recoverability. The recoverability test of CO_2 adsorption–desorption onto of Fe-GCAC/800 is consistent with the results obtained in the isosteric heat calculation of adsorption. With the present study, we propose a simple and low-cost method to produce highly efficient AC with a high surface area for CO_2 and CH_4 adsorption.

Acknowledgments

B.Z. Büyükbekar partially contributed from his PhD thesis and he thanks Selçuk University Scientific Research Council (project number: 18201081). The authors also would like to thank the Selçuk University Advanced Technology Research and Application Center for the facilities and technical assistance.

References

1. WMO. The State of Greenhouse Gases in the Atmosphere Based on Global Observations through 2015. World Meteorological Organization. 2016.
2. He, J. J.; To, J. W. F.; Psarras, P. C.; Yan, H. P.; Atkinson, T.; Holmes, R. T.; Nordlund, D.; Bao, Z. N.; Wilcox, J. *Adv. Energy Mater.* **2016**, *6*, 1502491.
3. Plaza, M. G.; Gonzalez, A. S.; Rubiera, F.; Pevida, C. *J. Chem. Technol. Biot.* **2015**, *90*, 1592-1600.
4. Fujiki, J.; Chowdhury, F. A.; Yamada, H.; Yogo, K. *Chem. Eng. J.* **2017**, *307*, 273-282.
5. Heidari, A.; Younesi, H.; Rashidi, A.; Ghoreyshi, A. A. *Chem. Eng. J.* **2014**, *254*, 503-513.
6. Sarici-Ozdemir, C.; Onal, Y. *Particul. Sci. Technol.* **2018**, *36*, 254-261.
7. Royer, B.; Cardoso, N. F.; Lima, E. C.; Vaghetti, J. C. P.; Simon, N. M.; Calvete, T. *J. Hazard. Mater.* **2009**, *164*, 1213-1222.
8. Wickramaratne, N. P.; Jaroniec, M. *ACS Appl. Mater. Interfaces* **2013**, *5*, 1849-1855.
9. Baccar, R.; Bouzid, J.; Feki, M.; Montiel, A. *J. Hazard. Mater.* **2009**, *162*, 1522-1529.
10. Namasivayam, C.; Kadirvelu, K. *Carbon* **1999**, *37*, 79-84.
11. Zhang, Q. L.; Lin, Y. C.; Chen, X.; Gao, N. Y. *J. Hazard. Mater.* **2007**, *148*, 671-678.
12. Mohan, D.; Sarswat, A.; Singh, V. K.; Alexandre-Franco, M.; Pittman, C. U. *Chem. Eng. J.* **2011**, *172*, 1111-1125.
13. Sarici-Ozdemir, C.; Kilic, F. *Particul. Sci. Technol.* **2018**, *36*, 194-201.
14. Sarici-Ozdemir, C.; Onal, Y.: Akmil-Basar, C. *Fuel Process. Technol.* **2006**, *87*, 979-986.
15. Kante, K.; Nieto-Delgado, C.; Rangel-Mendez, J. R.; Bandosz, T. J. *J. Hazard. Mater.* **2012**, *201*, 141-147.
16. Xiao, J.; Ma, X. L.; Song, C. S.; Li, Z. *Abstr. Pap. Am. Chem. Soc.* **2009**, *238*.
17. Laksaci, H.; Khelifi, A.; Trari, M.; Addoun, A. *J. Clean Prod.* **2017**, *147*, 254-262.
18. Kirbiyik, C.; Putun, A. E.; Putun E. *Water Sci. Technol.* **2016**, *73*, 423-436.
19. Kirbiyik, C.; Kilic, M.; Cepeliogullar, O.; Putun, A. E. *Water Sci. Technol.* **2012**, *66*, 231-238.
20. Hong, S. M.; Jang, E.; Dysart, A. D.; Pol, V. G.; Lee, K. B. *Sci. Rep.* **2016**, *6*, 34590.
21. Younas, M.; Leong, L. K.; Mohamed, A. R.; Sethupathi, S. *Chem. Eng. Commun.* **2016**, *203*, 1455-1463.
22. Abbas, M.; Kaddour, S.; Trari, M. *J. Ind. Eng. Chem.* **2014**, *20*, 745-751.
23. Tseng, R. L.; Wu, F. C.; Juang, R. S. *Sep. Purif. Technol.* **2015**, *140*, 53-60.
24. Creamer, A. E.; Gao, B.; Zhang, M. *Chem. Eng. J.* **2014**, *249*, 174-179.
25. Hulicova-Jurcakova, D.; Kodama, M.; Shiraishi, S.; Hatori, H.; Zhu, Z. H.; Lu, G. Q. *Adv. Funct. Mater.* **2009**, *19*, 1800-1809.
26. Togashi, T.; Naka, T.; Asahina, S.; Sato, K.; Takami, S.; Adschiri, T. *Dalton Trans.* **2011**, *40*, 1073-1078.
27. Song, M.; Jin, B. S.; Xiao, R.; Yang, L.; Wu, Y. M.; Zhong, Z. P. *Biomass Bioenergy* **2013**, *48*, 250-256.
28. Hao, W.; Björkman, E.; Lilliestråle, M.; Hedin, N. *Appl. Energy* **2013**, *112*, 526-532.
29. Younas, M.; Leong, L. K.; Mohamed, A. R.; Sethupathi, S. *Chem. Eng. Commun.* **2016**, *203*, 1455-1463.
30. Shahkarami, S.; Dalai, A. K.; Soltan, J. *Ind. Eng. Chem. Res.* **2016**, *55*, 5955-5964.
31. Hong, S. M.; Jang, E.; Dysart, A. D.; Pol, V. G.; Lee, K. B. *Sci. Rep.* **2016**, *6*, 34590.
32. Zhang, C.; Song, W.; Sun, G.; Xie, L.; Wang, J.; Li, K.; Sun, C.; Liu, H.; Snape, C. E.; Drage, T. *Energy Fuels* **2013**, *27*, 4818-4823.
33. Shahkarami, S.; Dalai, A. K.; Soltan, J. *Ind. Eng. Chem. Res.* **2016**, *55*, 5955-5964.
34. Sahin, O.; Saka, C.; Ceyhan, A. A.; Baytar, O. *Sep. Sci. Technol.* **2015**, *50*, 886-891.
35. Islam, M. A.; Ahmed, M. J.; Khanday, W. A.; Asif, M.; Hameed, B. H. *Ecotoxicol. Environ. Saf.* **2017**, *138*, 279-285.

36. Arami-Niya, A.; Rufford, T. E.; Zhu, Z. *Energy Fuels* **2016**, *30*, 7298-7309.
37. Park, H. J.; Suh, M. P. *Chem. Sci.* **2013**, *4*, 685-690.
38. Yang, Q.; Xu, Q.; Liu, B.; Zhong, C.; Berend, S. *Chinese J. Chem. Eng.* 2009, *17 (5)*, 781-790.
39. Plaza, M. G.; González, A. S.; Pevida, C.; Pis, J. J.; Rubiera, F. *Appl. Energy* **2012**, *99*, 272-279.
40. Plaza, M. G.; Pevida, C.; Arias, B.; Fermoso, J.; Casal, M. D.; Martín, C. F.; Rubiera, F.; Pis, J. J. *Fuel* **2009**, *88*, 2442-2447.
41. Gonzáles, A. S.; Plaza, M. G.; Rubiera, F.; Pevida, C. *Chem. Eng. J.* **2013**, *230*, 456-465.
42. Shahkarami, S.; Azargohar, R.; Dalai, A. K.; Soltan, J. *J. Environ. Sci.* **2015**, *34*, 68-76.
43. Plaza, M. G.; Pevida, C.; Martín, C. F.; Fermoso, J.; Pis, J. J.; Rubiera, F. *Sep. Purif. Technol.* **2010**, *71*, 102-106.
44. Zhang, Z.; Wang, K.; Atkinson, J. D.; Yan, X.; Li, X.; Rood, M. J.; Yan, Z. *J. Hazard. Mater.* **2012**, *229*, 183-191.
45. Blanco, A. A. G.; de Oliveira, J. C. A.; López, R.; Moreno-Piraján, J. C.; Giraldo, L.; Zgrablich, G.; Sapag, K. *Colloids Surf. A Physicochem. Eng. Asp.* **2010**, *357*, 74-83.
46. Himeno, S.; Komatsu, T.; Fujita, S. *J. Chem. Eng. Data* **2005**, *50*, 369-376.
47. Pevida, C.; Drage, T. C.; Snape, C. E. *Carbon* **2008**, *46*, 1464-1474.
48. Álvarez-Gutiérrez, N.; Gil, M.; Martínez, M.; Rubiera, F.; Pevida, C. *Energies* **2016**, *9*, 189.
49. Li, K.; Tian, S.; Jiang, J.; Wang, J.; Chen, X.; Yan, F. *J. Mater. Chem. A* **2016**, *4*, 5223-5234.
50. Jackson, K. T.; Rabbani, M. G.; Reich, T. E.; El-Kaderi, H. M. *Polym. Chem.* **2011**, *2*, 2775-2777.
51. Almansa, C.; Molina-Sabio, M.; Rodríguez-Reinoso, F. *Micropor. Mesopor. Mater.* **2004**, *76*, 185-191.
52. Andres, J. M.; Orjales, L.; Narros A.; Fuente, M. M.; Rodrigues, M. E. *J. Air Waste Manag. Assoc.* **2013**, *63*, 557-564.
53. Manusamy, K.; Somani, R. S.; Bajaj, H. C. *J. Environ. Chem. Eng.* **2015**, *3*, 2750-2759.
54. Wang, J.; Heerwig, A.; Lohe, M. R.; Oschatz, M.; Borchardt, L.; Kaskel, S. *J. Mater. Chem.* **2018**, *22*, 13911-13913.
55. Reddy, P. M. K.; Krushnamurty, K. Mahammadunnisa, S. K. Dayamani, A. Subrahmanyam C. *Int. J. Environ. Sci. Technol.* **2015**, *12*, 1363-1372.
56. Alvarez-Gutierrez, N.; García S.; Gil M. V., Rubiera F.; Pevida C. *Energy Fuels* **2016**, *30*, 5005-5015.
57. Zhang, Z.; Zhang, W.; Chen, X.; Xia, Q.; Li, Z. *Sep. Sci. Technol.* **2010**, *45*, 710-719.
58. Wang, Y. X.; Liu, B. S.; Zheng, C. *J. Chem. Eng. Data* **2010**, *55*, 4669-4676.
59. Hao, W.; Björnerbäck, F.; Trushkina, Y.; Oregui-Bengoechea, M.; Salazar-Alvarez, G.; Barth, T.; Hedin, N. *ACS Sustain. Chem. Eng.* **2017**, *5*, 3087-3095.
60. Choma, J.; Stachurska, K.; Marszewski, M.; Jaroniec, M. *Adsorption* **2016**, *22*, 581-588.
61. Awadallah, A.; Al-Muhtaseb, S. A. *Adsorption* **2013**, *19*, 967-977.
62. Khalili, S.; Khoshandam, B.; Jahanshahi, M. *Korean J. Chem. Eng.* **2016**, *33*, 2943-2952.
63. Mofarahi, M.; Gholipour, F. *Micropor. Mesopor. Mat.* **2014**, *200*, 1-10.
64. Wei, J.; Zhou, D.; Sun, Z.; Deng, Y.; Xia, Y.; Zhao, D. *Adv. Funct. Mater.* **2013**, *23*, 2322-2328.
65. Ning, P.; Li, F. R.; Yi, H. H.; Tang, X. L.; Peng, J. H.; Li, Y. D.; He, D.; Deng, H. *Sep. Purif. Technol.* **2012**, *98*, 321-326.
66. Ribeiro, R. P.; Sauer, T. P.; Lopes, F. V.; Moreira, R. F.; Grande, C. A.; Rodrigues, A. E. *J. Chem. Eng. Data* **2008**, *53*, 2311-2317.
67. Lopes, F. V. S.; Grande, C. A.; Ribeiro, A. M.; Loureiro, J. M.; Evaggelos, O.; Nikolakis, V.; Rodrigues, A. E. *Sep. Sci. Technol.* **2009**, *44*, 1045-1073.
68. Kemp, K. C.; Baek, S. B.; Lee, W. G.; Meyyappan, M.; Kim, K. S. *Nanotechnology* **2015**, *26*, 385602.
69. Boyjoo, Y.; Cheng, Y.; Zhong, H.; Tian, H.; Pan, J.; Pareek, V. K.; Jiang, S. P.; Lamonier, J. F.; Jaroniec, M.; Liu, J. *Carbon* **2017**, *116*, 490-499.